Study on Different Representations of Contrast for Inverse Scattering Problems

Tiantian Yin, Zhun Wei and Xudong Chen
Department of Electrical and Computer Engineering
National University of Singapore
Singapore
e0021489@u.nus.edu, a0096062@u.nus.edu, elechenx@nus.edu.sg

***Abstract*— In wavelet transform subspace-based optimization method (WT-SOM), full natural pixel bases are used to represent contrast. In this paper, the performance of representing contrast using full natural pixel bases and truncated wavelet bases is compared. In our simulations, it is found that using truncated wavelet bases for the representation of contrast has similar convergence rate compared to using full natural pixel bases. Compared to using full natural pixel bases, using truncated wavelet bases requires additional discrete wavelet transform to be done in each loop. Therefore, representing contrast using natural pixel bases is a better choice than using truncated wavelet bases.**

Keywords—wavelet bases, optimization, inverse scattering

I. INTRODUCTION

Inverse scattering problems have been widely used in different areas, such as detecting defects [1], microwave tomography [2]. However, they are difficult to solve due to ill-conditionness and non-linearity.

Wavelet bases are popular in solving inverse scattering problems since it can decrease the number of unknowns in the inverse problem and reconstruct profiles with multiresolution. In [1], wavelet bases are used to represent the contrast, the computational cost of inversion method can be greatly reduced by only using the wavelet bases localized within the area where the defects are located. When the background is lossy [3], the wavelet bases can be truncated so that the profile can be reconstructed with higher resolution in the area where more information is collected. Truncated wavelet bases have also been used to represent induced current with better performance than using natural pixels bases [4]. In compressive sensing (CS), wavelet bases can be used to reconstruct targets which are not sparse with respect to natural pixel bases [5, 6].

Inspired by the previous works [7, 8], WT-SOM [9] uses wavelet bases to represent minor part of induced current. It is found that Daubechies 20 wavelet bases and Fourier bases have similar compressive property in representing minor part of induced current. When a strong scatterer is reconstructed, truncated wavelet bases or truncated Fourier bases could be used to represent minor part of induced current at the initial stage to improve the convergence rate of the inverse algorithm [7].

In this paper, the performance of representing the contrast using full natural pixel bases and truncated wavelet bases in WT-SOM is compared. It is shown that using truncated D20 wavelet bases for representation of contrast has similar performance with using full natural pixel bases. Without doing additional discrete wavelet transform in each loop, representing contrast using natural pixel bases is a better choice than using truncated wavelet bases.

II. FOURMULATION

In the 2D problems, there are four kinds of wavelet coefficients including approximation coefficients, horizontal, vertical and diagonal detail coefficients. At the *j*-level, they are calculated as:

$$a_{m,n}^{j}=\left(\left(V_m^j\right)^T\cdot V_n^j\right)\circ f \tag{1}$$

$$h_{m,n}^{j}=\left(\left(W_m^j\right)^T\cdot V_n^j\right)\circ f \tag{2}$$

$$v_{m,n}^{j}=\left(\left(V_m^j\right)^T\cdot W_n^j\right)\circ f \tag{3}$$

$$d_{m,n}^{j}=\left(\left(W_m^j\right)^T\cdot W_n^j\right)\circ f\ , \tag{4}$$

where f is the function in the spatial domain. V and W are the 1D scaling signal and wavelet respectively. m and n are the indexes of position.

The corresponding average and detail signals in the spatial domain are:

$$\begin{aligned}A^j=&a_{1,1}^{j}\left(\left(V_1^j\right)^T\cdot V_1^j\right)+\ldots+a_{1,n}^{j}\left(\left(V_1^j\right)^T\cdot V_n^j\right)\\&\ldots+a_{m,1}^{j}\left(\left(V_m^j\right)^T\cdot V_1^j\right)+\ldots+a_{m,n}^{j}\left(\left(V_m^j\right)^T\cdot V_n^j\right)\end{aligned} \tag{5}$$

$$\begin{aligned}H^j=&h_{1,1}^{j}\left(\left(W_1^j\right)^T\cdot V_1^j\right)+\ldots+h_{1,n}^{j}\left(\left(W_1^j\right)^T\cdot V_n^j\right)\\&\ldots+h_{m,1}^{j}\left(\left(W_m^j\right)^T\cdot V_1^j\right)+\ldots\_+h_{m,n}^{j}\left(\left(W_m^j\right)^T\cdot V_n^j\right)\end{aligned} \tag{6}$$

$$\begin{aligned}V^j=&v_{1,1}^{j}\left(\left(V_1^j\right)^T\cdot W_1^j\right)+\ldots+v_{1,n}^{j}\left(\left(V_1^j\right)^T\cdot W_n^j\right)\\&\ldots+v_{m,1}^{j}\left(\left(V_m^j\right)^T\cdot W_1^j\right)+\ldots+v_{m,n}^{j}\left(\left(V_m^j\right)^T\cdot W_n^j\right)\end{aligned} \tag{7}$$

$$\begin{aligned}D^j=&h_{1,1}^{j}\left(\left(W_1^j\right)^T\cdot W_1^j\right)+\ldots h_{1,n}^{j}\left(\left(W_1^j\right)^T\cdot W_n^j\right)\\&\ldots+h_{m,1}^{j}\left(\left(W_m^j\right)^T\cdot W_1^j\right)+\ldots+h_{m,n}^{j}\left(\left(W_m^j\right)^T\cdot W_n^j\right)\ .\end{aligned} \tag{8}$$

The cost function of WT-SOM is:

$$F(\bar{\alpha}_1,\bar{\alpha}_2,...,\bar{\alpha}_{Ni},\bar{\kappa}) = \sum_{p=1}^{Ni}\left(\frac{\|\bar{\delta}_{dat}\|^2}{\|\bar{E}_p^s\|^2}+\frac{\|\bar{\delta}_{sta}\|^2}{\|\bar{J}_p^+\|^2}\right)$$
$$= \sum_{p=1}^{Ni}\left(\frac{\|\bar{\bar{G}}_s W^{-1}(\bar{\alpha}_p)+\bar{\bar{G}}_s\cdot\bar{J}_p^+-\bar{E}_p^s\|^2}{\|\bar{E}_p^s\|^2}+\frac{\|\bar{\bar{A}}\cdot\bar{\alpha}_p-\bar{B}_p\|^2}{\|\bar{J}_p^+\|^2}\right), \quad (9)$$

where

$$\bar{\bar{A}}\cdot\bar{\alpha}_p = W^{-1}(\bar{\alpha}_p)-\bar{\chi}\cdot\bar{\bar{G}}_d\cdot W^{-1}(\bar{\alpha}_p)\ , \quad (10)$$

and

$$\bar{B}_p = \bar{\chi}\cdot(\bar{E}_p^{\,i}+\bar{\bar{G}}_d\cdot\bar{J}_p^{\,+})-\bar{J}_p^{\,+}\ . \quad (11)$$

The cost function of WT-SOM is similar to the cost function of SOM except that $\bar{\alpha}_p$ contains the wavelet coefficients used to represent the minor part of the induced current in the *p*th incidence in WT-SOM. W^{-1} means inverse discrete wavelet transform. The cost function is minimized using the conjugate gradient method.

III. Numericcal Results

In the setup of the simulations, the domain of interests (DOI) has a size of $2\times 2\ \mathrm{m}^2$ and 64×64 pixels after discretization. It is centered at the origin point. 32 receiving antennas are employed. They uniformly form a circle and are all 3 m away from the origin. The frequency of all the incidences is equal to 400 MHz. The "Austria" profile with relative permittivity equal to 2.3 is used. 10% additive Gaussian white noise (AWGN) has been added to the scattered fields. Relative error is defined to be the normalized root-mean-square error (RMSE) between reconstructed and exact profiles.

In the simulations, full bases contain 4096 bases. 256 bases which are the second level approximation coefficients are used to represent the minor part of the induced current. In the first case, the contrast is represented using second level approximation coefficients of D20 wavelet. In the second case, the contrast is represented using full natural pixel bases. In Fig. 1, we see the convergence rates of this two cases are almost the same. In Fig. 2, it is shown that the reconstructed profiles under the two cases after 300 iterations look similar. It might be due to the reason that the number of unknowns in contrast is much smaller than the number of unknowns in minor part of induced current. The number of bases representing contrast may not have much effect on the convergence rate of inverse algorithm compared to the number of bases representing minor part of induced current.

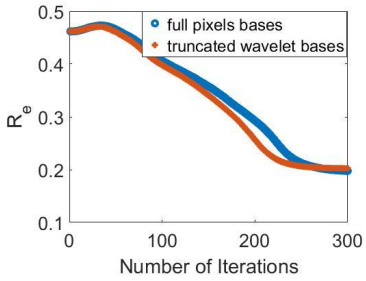

Fig. 1. Comparison of relative error in the first 300 iterations for different bases used to represent the contrast.

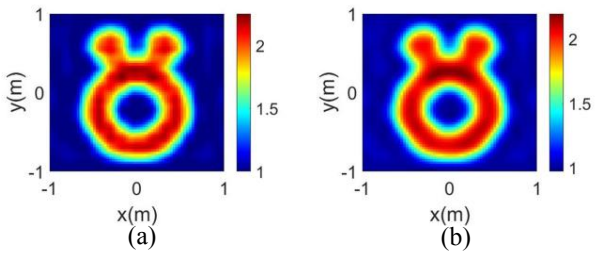

Fig. 2. Reconstructed relative permittivity profiles after 300 iterations using (a) truncated wavelet bases (256 bases) in wavelet domain for representation of the contrast, (b) full bases (4096 bases) in spatial domain for representation of the contrast.

IV. Conclusion

In this paper, it is found that using truncated wavelet bases has similar convergence rate compared to using full natural pixel bases for representation of contrast in WT-SOM. Since representing contrast using truncated wavelet bases requires additional discrete wavelet transform in each loop, using full natural bases is a better choice.

Acknowledgment

This research was supported by the National Research Foundation, Prime Minister's Office, Singapore under its Competitive Research Program (CRP Award No. NRF-CRP15-2015-03) and Temasek Lab@NUS Seed Research Project.

References

[1] O. Bucci, L. Crocco, T. Isernia *et al.*, "An adaptive wavelet-based approach for non-destructive evaluation applications," in *Proc. IEEE Antennas and Propagation Symp.*, 2000, pp. 1756-1759.

[2] I. Catapano, L. Di Donato, L. Crocco *et al.*, "On quantitative microwave tomography of female breast," *Prog. Electromagn. Res.,* vol. 97, pp. 75-93, 2009.

[3] O. M. Bucci, L. Crocco, T. Isernia *et al.*, "Subsurface inverse scattering problems: quantifying, qualifying, and achieving the available information," *IEEE Trans. Geosci. Remote Sens.,* vol. 39, no. 11, pp. 2527-2538, 2001.

[4] M. Li, O. Semerci, and A. Abubakar, "A contrast source inversion method in the wavelet domain," *Inverse Probl.,* vol. 29, no. 2, pp. 1-19, 2013.

[5] N. Anselmi, G. Oliveri, M. A. Hannan *et al.*, "Color compressive sensing imaging of arbitrary-shaped scatterers," *IEEE Trans. Microwave Theory Tech.,* vol. 65, no. 6, pp. 1986-1999, 2017.

[6] N. Anselmi, M. Salucci, G. Oliveri *et al.*, "Wavelet-based compressive imaging of sparse targets," *IEEE Trans. Antennas Propag.,* vol. 63, no. 11, pp. 4889-4900, 2015.

[7] X. Chen, "Subspace-based optimization method for solving inverse-scattering problems," *IEEE Trans. Geosci. Remote Sens.,* vol. 48, no. 1, pp. 42-49, 2010.

[8] Z. Wei, R. Chen, H. Zhao *et al.*, "Two FFT Subspace-Based Optimization Methods for Electrical Impedance Tomography," *Prog. Electromagn. Res.,* vol. 157, pp. 111-120, 2016.

[9] T. Yin, Z. Wei, and X. Chen, "Wavelet Transform Subspace-Based Optimization Method for Inverse Scattering," *IEEE Journal on Multiscale and Multiphysics Computational Techniques,* vol. 3, pp. 176-184, 2018.